ELSEVIER

Chemical Geology 237 (2007) 401–417

CHEMICAL GEOLOGY
INCLUDING
ISOTOPE GEOSCIENCE

www.elsevier.com/locate/chemgeo

Geochemical variations between the 79 AD and 1944 AD Somma–Vesuvius volcanic products: Constraints on the evolution of the hydrothermal system based on fluid and melt inclusions

Annamaria Lima [a,*], Benedetto De Vivo [a], Luca Fedele [a], Francesca Sintoni [a,b], Alfonsa Milia [c]

[a] *Università di Napoli "Federico II", Dipartimento di Scienze della Terra, Via Mezzocannone, 8. 80138, Napoli, Italy*
[b] *Departement of Earth and Planetary Sciences, American Museum of Natural History, New York, NY 10024-5192, USA*
[c] *Istituto per l'Ambiente Marino Costiero-IAMC, Calata Porta di Massa, Porto di Napoli 80133, Napoli, Italy*

Accepted 29 July 2006

Editor: R.L. Rudnick

Abstract

A variety of metamorphic and metasomatized sedimentary nodules and cumulate ejecta are commonly present in Somma–Vesuvius pyroclastic products. In this paper we present compositional data for homogenized silicate melt inclusions (HMI) in olivine and clinopyroxene from cumulate nodules ejected by the 79 AD plinian and the 1944 AD interplinian eruptions. Variation diagrams of element ratios as a function of host crystal Mg# serve to constrain magma compositional variations. In addition HMI compositions in olivines and clinopyroxenes from nodules and volcanic rocks are compared with bulk rock compositions to examine the difference between "closed system" (MI) and "open-system" (bulk rocks) behaviour. Geochemical variations between 79 AD and 1944 AD samples are interpreted to represent the effects of hydrothermal processes active in the upper parts of the shallow magma chamber, before and during explosive plinian eruption. During 1944 AD interplinian activity, magmas continuously ascended through the system, undergoing simultaneous degassing and fractionation. The loosely cemented volcanic conduit does not allow significant build up of volatile pressure, leading to frequent, non-violent interplinian eruptions. The combination of ongoing magma supply and frequent eruptions results in near steady-state conditions under the volcano, which explains why there is such a small variation in the composition of the 1944 AD melt. A self-sealing process (as a result of precipitation of newly formed hydrothermal minerals) contributes to closing of the system at the end of the interplinian activity. Plinian explosive eruptions (e.g. 79 AD) occur after a long repose time under closed-conduit condition. This means that a carapace, surrounded by an impermeable rind, forms beneath the Somma–Vesuvius volcanic complex and around the upper portion of the shallow magma chamber, and is the interface between brittle and plastic rocks. Several different mechanisms may play a role in triggering major breaches of the sealed zone (e.g. the activation of a fault system after the 62 AD earthquake in the Somma–Vesuvius area). In 79 AD the local strain rate increased due to an upward surge of new magma to such a degree that previously plastic material underwent shear failure in response to a stress difference, causing an explosive eruption.

Keywords: Magmatic fluids; Self-sealing; Hydrothermal system; Hydrostatic and lithostatic pressure

* Corresponding author. Tel.: +39 081 2535058; fax: +39 081 2535070.
E-mail address: anlima@unina.it (A. Lima).

0009-2541/$ - see front matter © 2006 Published by Elsevier B.V.
doi:10.1016/j.chemgeo.2006.07.011

1. Introduction

Somma–Vesuvius is a Quaternary, silica-undersaturated, potassic to ultrapotassic eruptive center intruded into Meso- to Cenozoic carbonate sequences.

The volcano is intensely investigated by many research groups because it is one of the most potentially hazardous volcanoes in the world. Nevertheless although much is now known about the volcano and its magmatic processes, a comprehensive understanding of its complex magmatic system has not yet been achieved.

Somma–Vesuvius is a composite volcano located on the southwestern coast of the Campanian Plain (Fig. 1). The Campanian margin is a Middle Pleistocene half graben filled by depositional sequences that are arranged in succession sets that display long-term aggradational–progradational stacking patterns (Milia, 1999; Milia and Torrente, 1999). The Mesozoic–Cenozoic carbonate substrate, cropping out on the Sorrento Peninsula, dips towards the NW and is overlain by Quaternary sediments and volcanic products. The volcano lies above NW–SE normal faults that in the submarine counterpart control the cryptodome emplacement and gas emission (Milia et al., 1998; Bellucci et al., 2006).

Mt. Somma began its eruptive activity at least 35 ka BP (Scandone et al., 1993), but the first episode of volcanic activity within the Somma–Vesuvius area has been dated at 400 ka BP and occurred in a marine environment (Brocchini et al., 2001). According to

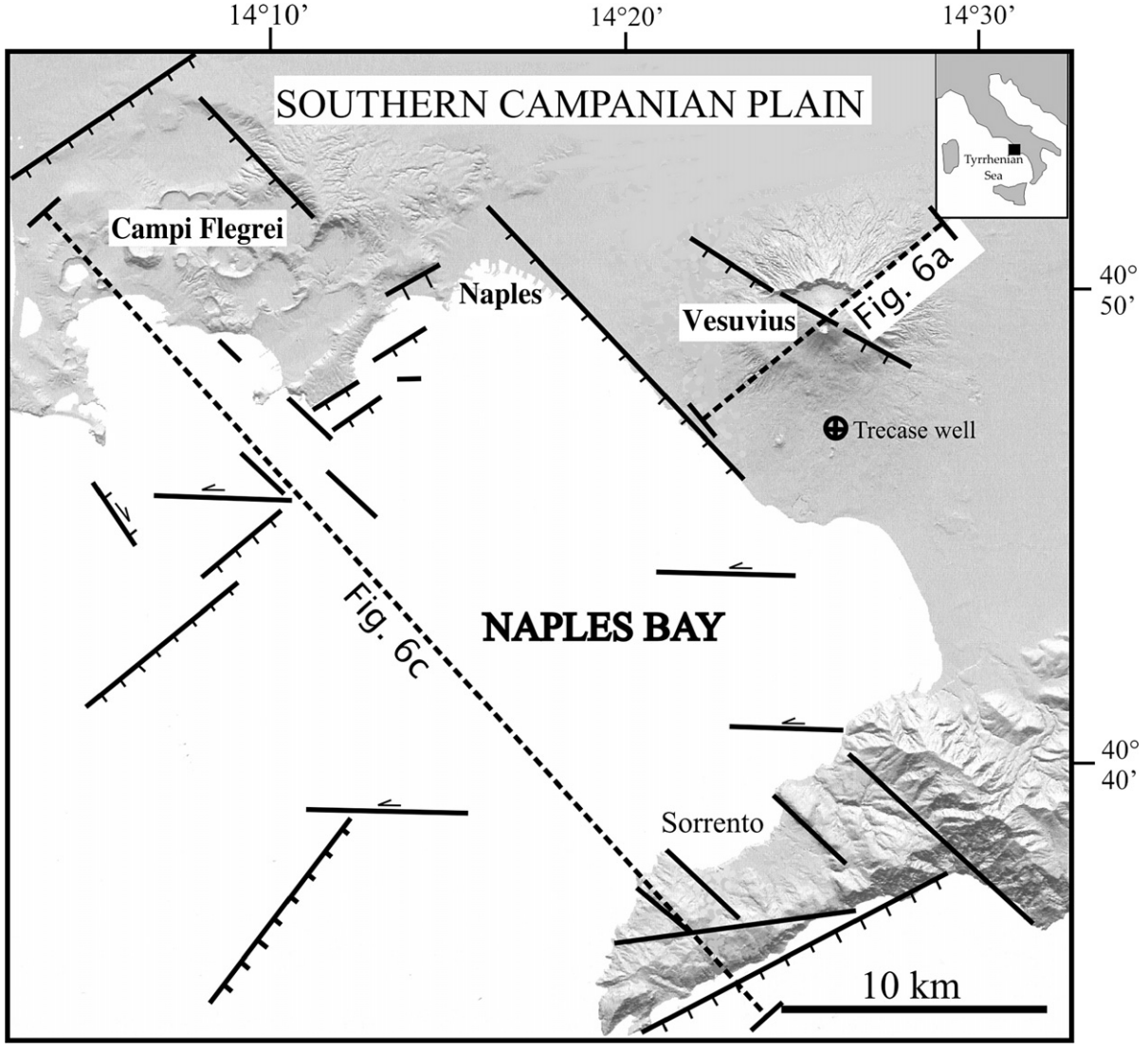

Fig. 1. Structural map of the Southern Campanian plain (from Milia and Torrente, 1999), also shown are the sections of Fig. 6.

Rolandi et al. (1998), the current Vesuvius cone was built by post-472 AD interplinian activity that followed the 472 AD subplinian eruption. Activity which can be attributed to the Mt. Somma system extends to as recent as 3.5 ka according to Webster et al. (2001).

The eruptive styles and cyclicity of the Somma–Vesuvius system have varied widely. The effusive lava flow and scoria eruptions were the most common type of volcanism during the last 3.5 ka, but they were periodically superseded by highly explosive plinian eruptions of pumice and ash, that also involved pyroclastic flows and surges.

Somma–Vesuvius products include basic, silica-undersaturated, potassic rocks, ranging from tephrite to phonolite, and less alkaline basaltic trachyandesites. Ayuso et al. (1998) have separated Somma–Vesuvius volcanics into three age groups characterized by a gradual change in composition. The three groups display distinct positive trends of alkalis versus silica, which become increasingly steeper with age. In the first group (from >25,000 yr B.P. to about 14,000 yr B.P) there is an increase in silica and alkalis with time, whereas an opposite tendency is observed in the two younger groups (from about 8000 yr B.P. to 2700 B.P. and from 79 A.D. to 1944 respectively).

Despite the significant efforts made to understand Somma–Vesuvius magmatism, the depth (and the internal physical parameters) of its magma chamber(s) remain uncertain. Using petrological and isotopic data, Santacroce et al. (1993) suggested that a single magma reservoir is located at a shallow depth within the limestone basement, whereas others, using isotopic and CO_2-rich fluid inclusion data, inferred the existence of two or more magma chambers (Cortini and Hermes, 1981; Belkin et al., 1985; Cortini et al., 1985; Belkin and De Vivo, 1993; Marianelli et al., 1999; Lima et al., 2003). High-resolution seismic tomography investigations did not resolve a shallow magma chamber, instead recent investigations identified a sharp transition to a low-velocity zone at >8 km, which may represent the top of a magma chamber (Zollo et al., 1998; Auger et al., 2001).

In this paper we present compositional data of homogenized silicate melt inclusions (HMI) in olivine and clinopyroxene from cumulate nodules ejected by the 79 AD plinian and the 1944 AD interplinian eruptions. Comparison of compositional data from HMIs in olivine and clinopyroxene from cumulate nodules with compositions of HMIs in the same minerals in the volcanics, and with bulk rock compositions have been carried out in order to examine differences between the "closed system" represented by HMIs and the "open-system" represented by bulk rocks.

2. Previous studies on Somma–Vesuvius nodules

Metamorphic and metasomatized sedimentary nodules, ranging from carbonates to silicic skarn rocks, and cumulate ejecta, commonly present in Vesuvius pyroclastic products, were originally described by Zambonini (1910). These nodules have been extensively studied by Hermes and Cornell (1978, 1981, 1983), Barberi and Leoni (1980) and Fulignati et al. (1998). Hermes and Cornell (1978) identified four varieties of nodule ejecta: 1) biotite-bearing pyroxenite, wehrlite, and dunite "accumulative" rocks; 2) "skarns", which are metasomatized carbonates; 3) recrystallized carbonate hornfels and 4) shallow plutonic rocks.

Several studies of fluid and melt inclusions (De Vivo et al., 1982; Belkin et al., 1985; Cortini et al., 1985; Belkin and De Vivo, 1993; Gilg et al., 1999; Fulignati et al., 2000a,b; Fulignati et al., 2001; Gilg et al., 2001; Lima et al., 2003; Fulignati et al., 2004) have been conducted to constrain the physical conditions of nodule genesis. Cortini et al. (1985) reported crystallization temperatures of 850–1050 °C for skarns and 1170–1240 °C for cumulate rocks based on MI studies. Belkin et al. (1985) studied nodules collected in interplinian volcanics and estimated that the nodules formed at 1–3.5 kbar based on densities of CO_2-rich fluid inclusions. The inclusions display a wide range of densities in a single rock, and sometimes in a single mineral. However, an important feature of the depth distribution is that it shows discrete groups, rather than a continuum, suggesting that these rocks underwent a multistage crystallization history. The multistage history is also indicated by Sr isotopes (Cortini and Hermes, 1981). The latter authors report that minerals of the cumulate rocks generally are in disequilibrium with each other with respect to Sr isotopes. This shows that these rocks equilibrated in different environments with distinct Sr isotopic compositions.

Belkin and De Vivo (1993) examined CO_2 fluid inclusions in clinopyroxene from cumulate and sub-effusive nodules from plinian eruptions. They report trapping depths between 1 and 2.5 kbar and also abundant H_2O-rich CO_2 fluid inclusions. They point out that such inclusions (H_2O-rich CO_2) are rare in non-plinian eruptions. According to Belkin and De Vivo (1993), fluid inclusions in plinian nodules record a higher pre-eruptive H_2O content of the magma.

Gilg et al. (2001) studied the mineralogy, fluid inclusions and C, O, Pb, Sr, and Nd isotopic compositions of skarn ejecta and associated xenolithic nodules. The Pb, Nd, C and O isotope compositions of skarn and the presence of silicate melt inclusion-bearing

wollastonite nodules indicates assimilation of carbonate wall rock by the alkaline magma at moderate depth (<5 km) which promoted exsolution of CO_2-rich vapor and complex saline melts from a locally contaminated magma. The main contributions from this study, for understanding the Somma–Vesuvius hydrothermal system, will be reported in the next section.

Lima et al. (2003) based on FI and MI, and on other petrologic data, suggest that the entire Somma–Vesuvius volcanic system resembles a complex feeding column which is dominated by multiple mush zone environments (small magma chambers), and thus includes a variety of local crystallization environments characterized by contrasting cooling rates and P–T conditions (Marsh, 1995). The shallower chamber with high aspect ratio should occur at a pressure of about 925–1000 bars (Belkin et al., 1985; Belkin and De Vivo, 1993). On the basis of petrography and mineral compositions, Lima et al. (2003) suggest that clinopyroxenes in cumulate nodules were formed at variable stages of fractionation of a single magmatic system.

Higher concentrations of volatile elements in MIs in more primitive phenocrysts imply that they crystallized at a higher pressure in a deeper magma chamber. The authors pointed out that the very tight major element compositional trends, formed by "basaltic" post-472 AD Vesuvius volcanic rocks, indicate that the composition of the erupting evolved melts has changed little since 472 AD, and that the magma chamber supplying post-472 AD interplinian eruptions is essentially in a steady-state condition. Interplinian volcanic rocks usually have higher MgO contents because their compositions reflect accumulation of clinopyroxene by a melt with ~4 wt.% MgO, whose composition remained unchanged since the 79 AD eruption. The similarity in composition of the plinian and interplinian bulk rocks with ~4 wt.% MgO suggests that during all Vesuvius post-79 AD eruptions the composition of the melt remained essentially the same.

Fulignati et al. (2004) argue that processes involved in skarn genesis at the walls of Vesuvian magma chambers are controlled by the characteristics of magma reservoirs. They indicate circulation of magmatic hypersaline fluid phases in the peripheral upper parts of the 79 AD and of 472 AD magma chambers. The magma chamber had a larger dimension in the 79 AD eruption. Segregation and migration of these hypersaline phases from crystallizing melts are responsible for endoskarn and exoskarn formation. Conversely, magmatic skarns are dominated by melt–solid diffusion processes. Fulignati et al. (2004) also support the idea that these xenoliths derive from margins of growing magma chambers and are not related to older magmatic reservoirs.

2.1. Previous studies of the Somma–Vesuvius hydrothermal system

Much of the information available on the Somma–Vesuvius hydrothermal system is derived from studies of skarn xenoliths. Skarns are Ca–Fe–Mg–Mn-rich silicate rocks formed by high-temperature metasomatic reactions mostly involving carbonate rocks (e.g. Einaudi et al., 1981). An aqueous fluid phase is always involved in such metasomatic reactions (e.g.Kwak, 1986; Meinert et al., 1997). At Somma–Vesuvius, skarn ejecta is characterized by a specific mineralogy that includes vesuvianite, wollastonite, anorthite, phlogopite, gehlenite, scapolite and clinopyroxene. Mineral zonation at the contact with the carbonate rocks is common in the plinian and subplinian eruption products. Skarn ejecta are potentially valuable sources of information to understand fluid evolution at magma chamber walls.

Gilg et al. (2001) calculated the pressure of skarn formation from the densities of CO_2 inclusions in wollastonite in skarn nodules. The results indicate trapping pressures from 660 to 1368 bars [assuming a formation temperature of ~1000 °C and using Brown and Lamb (1989) equation of state for CO_2]. Gilg et al. (2001) also calculated the salinity of multiphase aqueous brine inclusions of 43–52 wt.% NaCl equiv. with total homogenization temperatures ranging between 720–820 °C. Fulignati et al. (2004) calculate salinity in the range 62–66 wt.% NaCl equiv. and temperatures in the range 760–880 °C in skarn sampled from 79 AD volcanics. Saline–melt inclusions showing immiscibility between silicate and salt melt (Gilg et al., 1999) have salinities up to 55 wt.% NaCl equiv., with total homogenization temperatures ranging between 870–890 °C (Gilg et al., 2001). Fulignati et al. (2004) calculate salinities ranging between 52–80 wt.% NaCl equiv. and temperatures between 970–980 °C for the same type of inclusions of Gilg et al. (2001) from skarns of 79 AD volcanics.

Gilg et al. (2001) conclude that there is no evidence for a convectively cooling hydrothermal system at the magma–carbonate wall rock interface at Somma–Vesuvius, based on a lack of participation of externally derived fluids, such as meteoric waters or formational fluids. Chiodini et al. (2001) suggest that NaCl brines reside in the high temperature reservoir beneath Somma–Vesuvius volcano and influences the chemical composition of the gases discharged by the fumaroles of

Table 1
Representative EMPA analyses (wt.%) of homogenized silicate melt inclusions hosted in olivine and clinopyroxene phenocrysts from cumulate nodules sampled in 79 AD and 1944 AD volcanics

Sample	DV506								DV11			
Host mineral	Olivine				Clinopyroxene				Olivine			
Eruption	79 A.D.								1944 A.D.			
Label	5A-MI	3D-MI	4A-MI	6A-MI	6B-MI	4B-MI	6C-MI	7A-MI	2D-MI	3C-MI	3D MI	4B-MI
Trun °C	1130	1126	1082	1159	1159	1123	1123	1081	1133	1119	1131	1118
Tcalc. °C	1208	1213	1206	1227	1151	1176	1174	1154	1205	1193	1198	1214
Mg# host meas.	85.45	85.03	84.94	84.80	86.20	88.51	88.51	86.58	85.72	85.70	84.48	86.05
Mg# host calc.	85.97	85.60	84.85	84.49	81.10	87.28	89.05	84.06	84.74	84.37	84.81	86.65
SiO_2	47.94	47.09	45.75	47.68	48.03	46.35	48.06	46.24	44.88	47.06	46.39	46.19
TiO_2	1.01	1.08	1.19	0.88	1.16	1.05	0.86	0.99	1.12	0.81	0.90	0.94
Al_2O_3	14.05	14.01	13.46	13.17	14.08	13.45	14.35	14.52	14.53	15.45	14.80	14.68
FeO	8.02	7.85	8.13	9.98	9.24	6.73	5.84	7.84	8.48	8.71	8.47	7.88
MnO	0.14	0.15	0.08	0.17	0.22	0.10	0.14	0.16	0.16	0.24	0.14	0.14
MgO	7.05	6.63	6.32	8.03	5.80	6.37	6.57	6.01	6.40	6.59	6.68	7.09
CaO	10.48	9.36	9.86	10.39	10.96	10.52	11.51	11.21	10.11	10.74	10.58	10.68
Na_2O	2.02	1.62	1.88	1.99	1.30	2.01	2.03	2.01	1.78	1.87	1.65	1.70
K_2O	3.92	4.90	5.11	3.11	5.51	4.94	3.67	3.44	5.60	4.92	4.73	4.78
P_2O_5	1.00	0.79	0.92	0.96	0.94	0.79	1.04	0.95	0.95	0.91	0.90	0.90
SO_2	0.61	0.56	0.63	0.58	0.17	0.42	0.50	0.55	0.39	0.37	0.37	0.39
F	bdl	0.20	0.31	bdl*	0.09	0.24	bdl	bdl	0.24	bdl	bdl	bdl
Cl	0.54	0.38	0.42	0.52	0.31	0.42	0.56	0.57	0.44	0.62	0.63	0.55
–O═Cl, F	0.12	0.17	0.23	0.12	0.11	0.20	0.13	0.13	0.20	0.14	0.14	0.12
Total	96.64	94.45	93.83	97.32	97.69	93.21	95.00	94.34	94.88	98.16	96.07	95.81

FeO* represents total iron; Mg#=[100*atomic Mg/Mg+∑Fe]. Host crystal Mg# measured and calculated; quenching temperatures (Trun) and calculated liquidus temperatures (Tcalc.) of olivine and clinopyroxene are also shown. The calculated values represent liquidus temperatures of clinopyroxene and olivine for the analyzed HMIs compositions under anhydrous conditions and are accurate within 15 °C (Ariskin et al., 1993). All calculations have been performed using the software PETROLOG (Danyushevsky, 2001).
*bdl = below detection limit.

the bottom of the crater. During the present period of repose, geochemical evidence indicates that there was no input of fresh magma at shallow depths after the end of the last eruptive period (Chiodini et al., 2001; Lima et al., 2003).

3. Sample description and methods

New cumulate nodules have been sampled to carry out detailed analysis on MI: the sample DV506 was collected at Terzigno in the 79 AD volcanic products and sample DV11 was collected on the slopes of Vesuvius, in the products of the 1944 activity, where the occurrence of scoriae, lava fragments and xenoliths mark a significant increase of explosivity late in the eruptive event (Dolfi and Trigila, 1978).

Nodules were hand crushed in an agate mortar and the resulting material was sieved to extract the 0.5–2 mm grain fraction from which olivine and clinopyroxene phenocrysts were hand-picked, mounted into epoxy and doubly polished to be examined for the presence of MI. The majority of MIs range from 25 to 50 μm in size and were either re-crystallized or devitrified. In order to obtain homogeneous glass compositions from MIs that have undergone post-entrapment crystallization they have been homogenized, even if not always totally (see the detailed description of the theory of homogenization of MIs given in Roedder, 1979) and quenched in the laboratory (experiments were conducted according to the procedure described in Danyushevsky et al., 2000; Lima, 2000). Homogenization experiments have been carried out at the Department of Geosciences of Virginia Tech (Blacksburg, USA) using the Vernadsky heating stage (Sobolev and Slutskii, 1984). After quenching, single crystals were mounted with epoxy on transparent polycarbonate rods and polished according to the technique described by Thomas and Bodnar (2002) to expose homogenized MIs (HMIs). Inclusions were analyzed at the "Istituto di Geologia Ambientale e Geoingegneria" (CNR), Roma, Italy, with an automated Cameca SX-50 and at the United States Geological Survey (Reston, Virginia) on a JEOL JXA-8600 electron microprobe. Whenever the size allowed it, HMIs were analyzed in two different spots. Host phenocrysts were analyzed at distances of about 20 μm from MI.

On both electron probes, analytical conditions were 15 keV and 10 nA, with a fixed beam size of 10 μm. In each analytical run, alkalis were always measured first, and no correction has been made for Na loss. Test runs made on synthetic and natural glass standards prior to the beginning of the analysis showed no significant alkali migration under the specified analytical conditions. Relative one-sigma precision is estimated to be 1 to 2% for major elements and 5 to 10% for minor elements.

4. Results

Representative compositions of HMIs (in olivine and clinopyroxene) from nodule DV506, collected in 79 AD volcanics, and from nodule DV11 (in olivine), collected in 1944 AD volcanics are shown in Table 1. Olivine compositions in nodules collected in 79 AD and 1944 AD volcanic rocks range from $Fo_{84.6}$ to $Fo_{85.5}$ and from $Fo_{84.5}$ to Fo_{86}, respectively. Cumulus clinopyroxene in nodules in 79 AD volcanics is diopsidic and Mg# (calculated on total Fe) ranges from 86.6 to 88.8. Each host crystal was analyzed in two different spots, on opposite sides of the HMI; no compositional variation exceeding the accuracy of microprobe analysis has been noted between individual points in each grain.

All HMIs are characterized by low analytical totals. This is interpreted to reflect the presence of significant amounts of H_2O in the trapped melts. This interpretation is supported by secondary ion mass spectrometry (SIMS) analyses made on Somma–Vesuvius volcanics (Belkin et al., 1998; Cioni, 2000; Raia et al., 2000; Lima et al., 2003) which showed H_2O contents up to 6 wt.% in MI. Indirect support for moderate to high H_2O contents in the MIs is also evident from the calculated liquidus temperatures of olivine and clinopyroxene (Table 1).

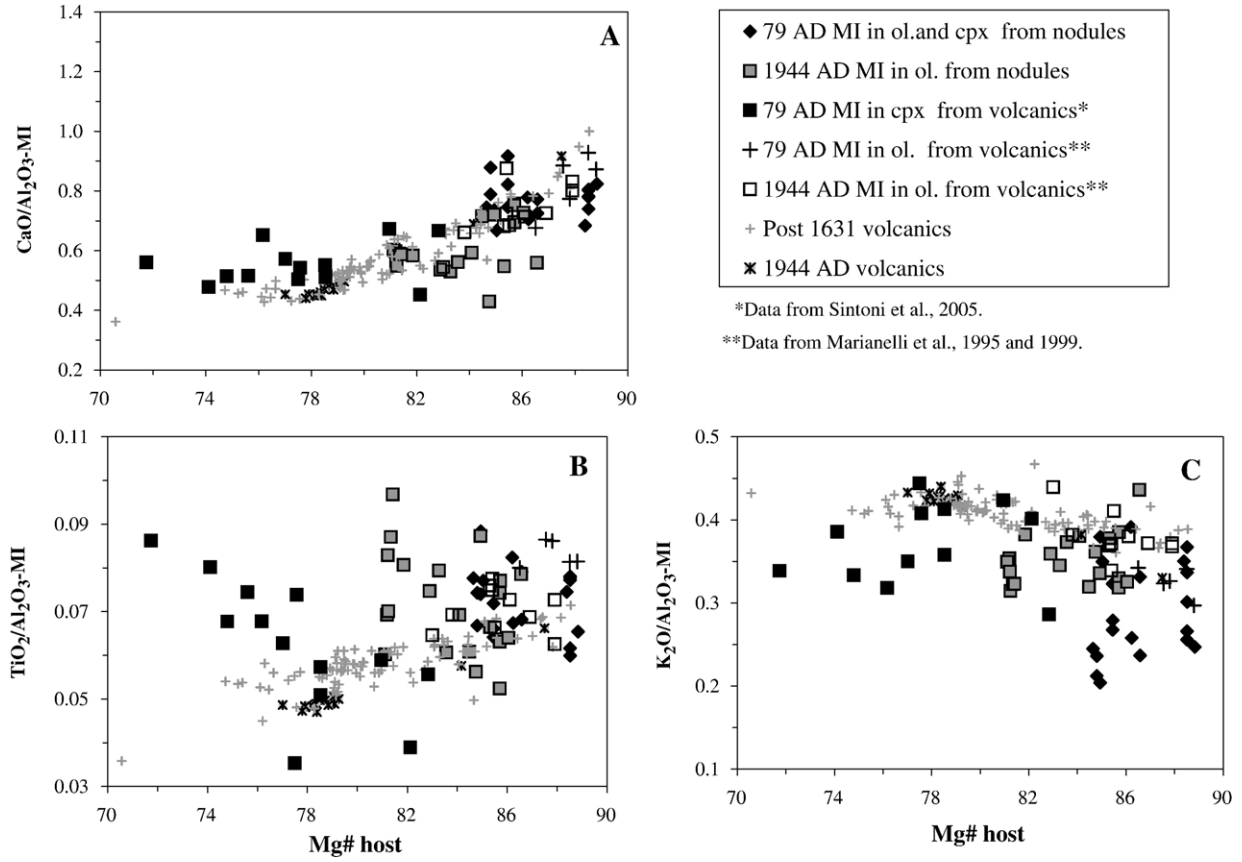

Fig. 2. Major-element compositions of HMIs in olivine and clinopyroxene from Somma–Vesuvius volcanics and nodules, plotted against Mg# of their host minerals. Also shown for comparison: post-1631 AD volcanic compositions (bulk rocks) (Ayuso et al., 1998); HMIs in clinopyroxene from 79 AD volcanics (Sintoni et al., 2005); MIs in olivine from 79 AD volcanics (Marianelli et al., 1995); MIs in olivine from 1944 AD volcanics (Marianelli et al., 1999). The compositions of the equilibrium olivine for each rock sample have been calculated using an olivine–melt equilibrium model of Ford et al. (1983), assuming an Fe^{2+}/Fe^{3+}value of 6. For Vesuvius compositions, this value corresponds to oxygen fugacity just below the NNO buffer. All calculations have been performed using the software PETROLOG (Danyushevsky, 2001).

The calculated values represent liquidus temperatures of clinopyroxene and olivine for the analyzed MI compositions under anhydrous conditions and are accurate within ±15 °C (Ariskin et al., 1993). Since H_2O is known to lower the liquidus temperatures of all anhydrous silicates, calculated anhydrous liquidus temperatures of the H_2O-bearing melts are higher than the actual liquidus temperatures (quenching temperature indicated as Trun in Table 1). The latter evidence indicates efficient quenching of MI. Calculated clinopyroxene and olivine compositions (indicated in Table 1 as Mg# host calc.) are generally similar to the measured ones (indicated in Table 1 as Mg# host meas.), implying that most MIs were not overheated during experiments (in overheated case host Mg# calculated should be higher than host Mg# measured). However, ratios of elements that are incompatible in the host, and also concentrations of elements that are present at similar levels in the melt and in the host (such as FeO* in inclusions in magnesian clinopyroxene and olivine, and TiO_2 and SiO_2 in inclusions in clinopyroxene), should not be affected significantly by over- or under-heating.

Variation diagrams for HMIs in olivine and clinopyroxene from cumulate nodule DV506 and HMIs in olivine from nodules DV11 and S3 are shown in Figs. 2 and 3. Olivine HMIs data from cumulate S3 nodule are from Lima et al. (2003). For comparative purposes, in the diagrams of Figs. 2 and 3 the following data have been considered: post-1631 AD volcanic compositions (bulk rocks) (Ayuso et al., 1998); HMIs in clinopyroxene from 79 AD volcanics (Sintoni et al., 2005); MIs in olivine from 79 AD volcanics (Marianelli et al., 1995); MIs in olivine from 1944 AD volcanics (Marianelli et al., 1999). To plot post-1631 AD interplinian volcanics shown in Figs. 2 and 3, the compositions of the equilibrium olivine for each rock sample have been calculated using the olivine-melt equilibrium model of Ford et al. (1983), assuming an Fe^{2+}/Fe^{3+} value of 6. For Vesuvius compositions, this value corresponds to an oxygen fugacity just below the NNO buffer.

The CaO/Al_2O_3 values of MIs in olivine and clinopyroxene from 79 AD and 1944 AD nodules and volcanics are shown in Fig. 2A. In general all MIs show decreasing CaO/Al_2O_3 values with decreasing host

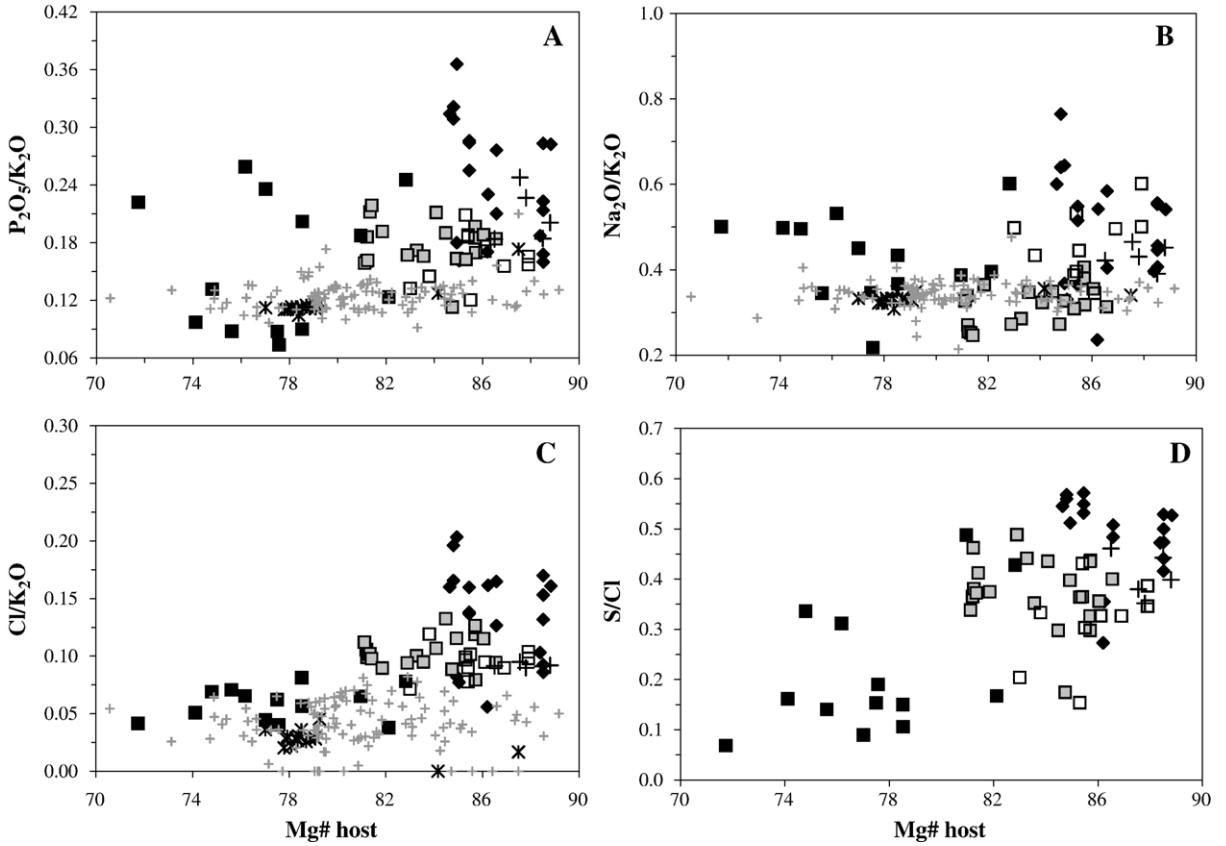

Fig. 3. Volatile element compositions of HMIs in 79 AD and 1944 AD olivine and clinopyroxene from Somma–Vesuvius cumulate nodules, plotted against host mineral Mg#. Symbols as in Fig. 2.

Table 2
P_2O_5/K_2O, Na_2O/K_2O, Cl/K_2O and S/Cl average values in cumulates olivine and clinopyroxene HMI, volcanic rock olivine and clinopyroxene HMIs and average volcanic bulk rock compositions

	Average value of:	79 A.D.	1944 A.D.
P_2O_5/K_2O	Mis in nodule o1° and cpx°	0.24 (0.06)	0.18 (0.01)
	Mis in volcanic o1° and cpx (I group)*	0.19 (0.04)	0.15 (0.03)
	Mis in volcanic cpx (II group)**	0.16 (0.07)	
	Volcanic compositions (b.r.°)***	0.02 (0.01)	0.12 (0.02)
Na_2O/K_2O	Mis in nodule ol and cpx	0.49 (0.12)	0.36 (0.03)
	Mis in volcanic ol and cpx (I group)*	0.40 (0.05)	0.39 (0.06)
	Mis in volcanic cpx (II group)**	0.43 (0.1)	
	Volcanic compositions (b.r.)***	0.54 (0.07)	0.33 (0.01)
Cl/K_2O	Mis in nodule ol and cpx	0.136 (0.041)	0.116 (0.017)
	Mis in volcanic ol and cpx (I group)*	0.099 (0.014)	0.089 (0.021)
	Mis in volcanic cpx (II group)**	0.061 (0.016)	
	Volcanic compositions (b.r.)***	0.068 (0.005)	0.024 (0.007)
S/Cl	Mis in nodule ol and cpx	0.52 (0.1)	0.36 (0.06)
	Mis in volcanic ol and cpx (I group)*	0.39 (0.7)	0.27 (0.06)
	Mis in volcanic cpx (II group)**	0.21 (0.1)	
	Volcanic compositions (b.r.)**	<0.05	<0.05

In parenthesis standard deviation; °Data from this study and Lima et al. (2003).
*Data from: (Marianelli et al. 1995, 1999; Raia et al. 2000; Webster et al., 2001).
**Data from Sintoni et al. (2005). ***Data from Ayuso et al. (1998).
°o1 = olivine, cpx = clinopyroxene, b.r. = bulk rocks.

mineral Mg#. This trend, as discussed by Lima et al. (2003), is consistent with olivine–clinopyroxene cotectic crystallization. Olivine and clinopyroxene HMIs from cumulate nodule (DV506) collected in 79 AD volcanics show less evolved compositions, with CaO/Al_2O_3 ratios varying in a more narrow range, with lower TiO_2/Al_2O_3 and K_2O/Al_2O_3 values (Fig. 2A–C) compared with HMIs in olivine from DV11 and S3 nodules, collected in 1944 AD volcanics. Olivine and clinopyroxene HMIs from 79 AD cumulate nodule also have the highest P_2O_5/K_2O, Na_2O/K_2O, Cl/K_2O and S/Cl contents (Fig. 3A–D).

Even if HMIs in olivine from 1944 nodules generally are in good agreement with MIs in olivine from 1944 volcanics, the latter have lower P_2O_5/K_2O, Cl/K_2O and S/Cl and higher Na_2O/K_2O ratios than HMIs in olivine from nodule collected in 1944 AD volcanics (Fig. 3A–D).

Olivine and clinopyroxene HMIs from 79 AD volcanics can be divided into Group I and Group II. Group I has compositions consistent with MIs in olivines and clinopyroxenes from 79 AD nodules; Group II vice versa has more evolved compositions, with much lower CaO/Al_2O_3 values, increasing TiO_2/Al_2O_3 ratios (Fig. 2B), decreasing K_2O/Al_2O_3 (Fig. 2C) and scattered P_2O_5/K_2O (Fig. 3A) ratios compared with correlative 79 AD nodule MIs. Group II HMIs have been trapped in more evolved 79 AD volcanic clinopyroxenes and in addition they have Na_2O/K_2O ratios comparable with olivine MIs in 1944 volcanics (Fig. 3B) but very low Cl/K_2O values – similar to >1631 volcanic bulk rock (Fig. 3C) – and S/Cl values (Fig. 3D).

Table 2 shows P_2O_5/K_2O, Na_2O/K_2O, Cl/K_2O and S/Cl average contents (in parenthesis 1 sigma precision) for HMIs from this study, for MIs previously plotted in Figs. 2 and 3 and also for 79 AD and 1944 AD MIs in clinopyroxenes from volcanics studied by Webster et al. (2001) and Raia et al. (2000). Note that in Table 2, HMIs in minerals from AD 79 volcanics have been organized in two groups because, as already pointed out, they represent two different populations. Group I HMIs have been averaged along with all MIs in minerals from volcanics (e.g. Marianelli et al., 1995; Webster et al., 2001), whereas Group II represents only Sintoni et al. (2005) data.

In Table 2, P_2O_5/K_2O values for the 79 AD samples vary from 0.24 in cumulate-hosted MIs to 0.19 (decrease of 21%) and to 0.16 (Group II with a decrease of 33%) in MIs from volcanic rock crystals with a strong decrease down to 0.02 (decrease of 88%) in bulk rock. The average P_2O_5/K_2O values for the 1944 AD interplinian samples vary from 0.18 in cumulate-hosted MIs to 0.15 in volcanics MIs (decrease of 17%), whereas a limited variation (20%) between MIs from volcanic rock crystals and bulk rock is observed. Average Na_2O/K_2O values vary in different ways. They decrease from 0.49 in cumulate-hosted MIs to 0.40 (18%) and to 0.43 (Group II with a decrease of 12%) in MIs from volcanic rock crystals and then increase to 0.54 (35%) in bulk rock. The average Na_2O/K_2O values for 1944 AD show only very weak variations from cumulate-hosted MIs (0.36) to MIs from volcanic rock crystals (0.39) to bulk rock composition (0.33) (increase and decrease of 8%, respectively). The average Cl/K_2O values for 79 AD decrease markedly from cumulate-hosted MIs (0.136) to MIs from volcanic rock crystals of Group II (0.061) (decrease of 55%); the latter has Cl/K_2O content slightly lower than bulk rock. The average Cl/K_2O values for 1944 AD interplinian decrease from 0.116 to 0.089 (23%) from cumulate-hosted MIs to MIs from volcanic rock crystals. Bulk rocks show a strong Cl/K_2O decrease,

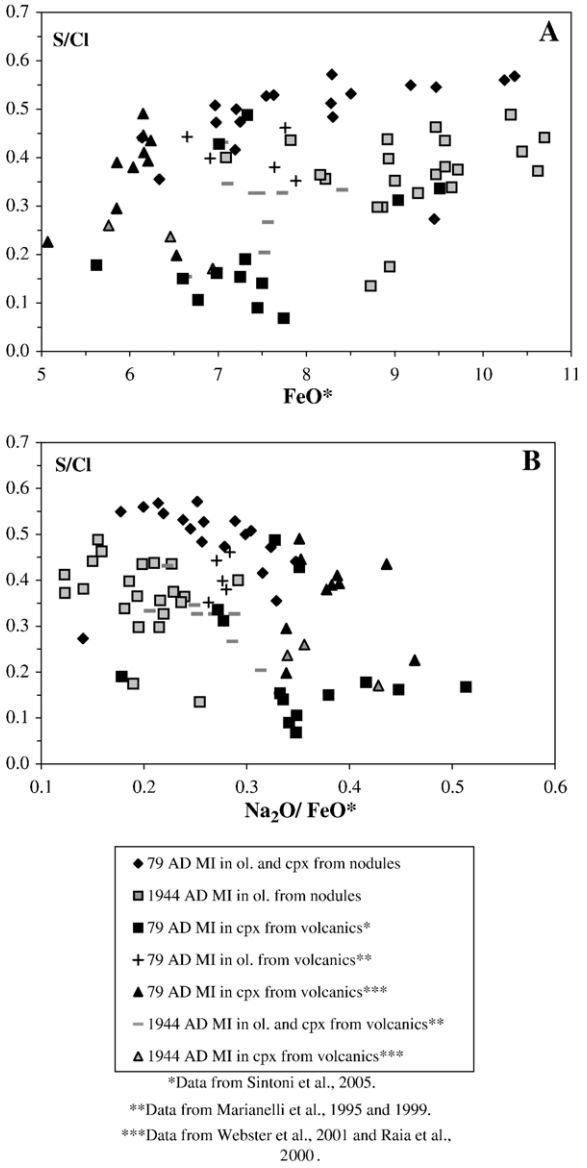

Fig. 4. A) S/Cl versus FeO* total iron and B) S/Cl versus Na_2O/FeO* in olivine and clinopyroxene MIs from AD 79 and 1944 cumulate nodules and volcanic rocks.

up to 0.024 (73%). Average S/Cl values can be compared only between cumulate and volcanic rocks MIs data. There is a decrease from 0.52 to 0.39 (Group I) to 0.21 (Group II) (25% and 60% respectively) for 79 AD and a decrease from 0.36 in cumulates MIs to 0.27 (25%) in volcanic crystals MIs for 1944 AD.

The 79 AD plinian cumulate MIs clearly display a higher S/Cl content compared with 1944 AD cumulate MIs (Fig. 3D). For HMIs, S/Cl values against FeO* (total iron) and NaO/FeO* are shown in Fig. 4; S/Cl ratio increases with increasing FeO* (Fig. 4A) and also with CaO and MgO (not shown) and decreases with increasing Na_2O/FeO* (Fig. 4B) and also with K_2O (not shown). In both diagrams (Fig. 4A and B), MIs from 79 AD plinian crystals show an evolutionary trend with a higher S/Cl ratio compared with MIs in 1944 AD interplinian crystals. These correlations do not reflect post-entrapment re-equilibration of MIs resulting in sulphide precipitation because there is no correlation between S and FeO* content of MIs.

5. Discussion

As shown in Figs. 2 and 3, HMIs in minerals from nodules display larger compositional variations compared with MIs in minerals from volcanics even if the general trend is always consistent with olivine–clinopyroxene cotectic crystallization. Particularly important is the finding that compositions of MIs in 79 AD volcanics represent two different population (named Group I and Group II).

Only HMIs in less evolved host crystals (Group I) have compositions consistent with 79 AD nodule HMIs. On the other hand plotting FeO* contents in MIs in olivine from the cumulate nodules versus Fo content of

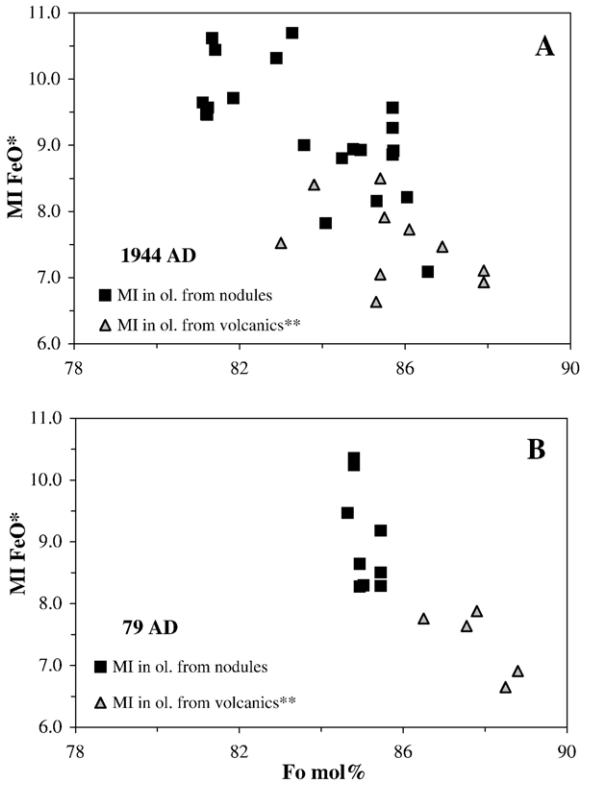

Fig. 5. Total iron (FeO*) in MIs versus Fo content of the host olivine for 79 AD (A) and for 1944 (B) MIs in nodules and volcanics.

the host olivine (Fig. 5), MIs in olivine from 79 AD nodules and from 79 AD volcanics Group I display (Fig. 5B) a similar trend to the ones shown by MIs in olivine from 1944 AD nodules and volcanics. As discussed by Danyushevsky et al. (2000), a negative correlation between FeO* contents in MIs and the Fo content of the host olivine (Fig. 5A and B), when observed in a magmatic series, results from post-trapping re-equilibration of MIs with their hosts at similar temperatures. The FeO* content of the residual melt inside MIs in olivine does not usually reflect its content in the trapped melt, but is a function of temporal variations in temperature after trapping (Danyushevsky et al., 2002), and it can be either lower or higher than the trapped value. Similar trend for MIs from the nodule DV11 and S3 and the host 1944 AD lava and for MIs from the nodule DV506 and host 79 AD volcanics indicate their common thermal evolution for some time prior to eruption.

The variation diagrams of volatile concentration as a function of host crystal Mg# selected here (Fig. 3A–D) reveal volatile variations in magma during olivine and clinopyroxene crystallization. Generally this type of diagram shows that olivine and clinopyroxene MIs from 79 AD plinian cumulate have a higher volatile content than olivine MIs from 1944 AD interplinian cumulate, even in host crystals showing the same Mg#.

Compositions of HMIs in olivine and clinopyroxene from cumulate nodule DV506 (sampled in 79 AD volcanics) and in olivine from nodules DV11 and S3 (sampled in 1944 AD volcanics) have been compared with compositions of HMIs in olivine and clinopyroxene from the 79 AD and 1944 AD volcanic rocks and with correlative 79 AD and 1944 AD bulk rock compositions (Table 2). The purpose of this comparison is to examine the possible different volatile trends between the "closed system" represented by MIs in crystals in nodules and volcanic rocks (even if MIs could represent partially degassed magma if the volatile phase or phases left the magmatic system) and the "open-system" behaviour expected for the bulk rock compositions.

Although nodule samples were collected in the same eruption where studied phenocrysts from volcanics were found, it is still important to determine when individual phenocrysts found in the ejecta formed or, alternatively, when MIs were trapped in phenocrysts. The best way to establish a relative chronology of MIs trapping is by evaluation of host crystal evolutionary trends (e.g. Mg#). As a consequence HMIs in less evolved crystals represent an earlier stage of magma evolution.

- The decreasing P_2O_5/K_2O ratio (Table 2 and Fig. 3A) from MIs in cumulate crystals to MIs in volcanic rock crystals for both 79 AD and 1944 AD, results from apatite crystallization that lowers the P concentration in the melt during magma evolution. Compared with bulk rock compositions, MIs in 1944 AD volcanic rock crystals show a week variation in P_2O_5/K_2O (there is a small difference between closed and open system behaviour). The large P_2O_5/K_2O depletion observed in 79 AD bulk rock (about 83% compared with 1944 AD bulk rock and 87.5% compared with P_2O_5/K_2O in MIs in 79 AD more evolved volcanic rock crystals, Group II) could be explained by hydrothermal fluids that (as discussed in the next paragraphs) deplete the magmatic system in P during magma ascent.
- The 1944 AD MIs and bulk rock compositions (Table 2 and Fig. 3B) show Na_2O/K_2O ratios that are very similar (difference is 8%). This implies that Na behaves as an incompatible element during magma fractionation. The increases of Na_2O/K_2O ratio in 79 AD bulk rock (~64% compared with 1944 AD bulk rock and ~35% to ~26% compared with 79 AD MIs Group I and II, respectively) imply that during magma ascent there was Na enrichment in the magmatic system (as discussed in the next paragraphs).
- MIs from the 79 AD and 1944 AD cumulate and volcanic crystals, and bulk rock compositions, show a progressive decrease in Cl/K_2O ratio (Table 2 and Fig. 3C). Somma–Vesuvius 79 AD and 1944 AD magmas were affected by Cl loss during their evolution. Bulk rock compositions from 1944 AD show a larger Cl/K_2O depletion compared with correlative MIs in volcanic crystals (~73%), vice versa Cl/K_2O content is quite the same in plinian 79 AD bulk rocks and in more evolved crystal MIs from AD 79 volcanics (Group II). This implies that removal of Cl was more efficient in pre-eruptive condition and/or during the 1944 AD interplinian eruption. On the other hand, Cl solubility is extremely sensitive to melt composition. Crystallization of Ca, Mg, Fe, and Al-rich minerals dramatically reduces Cl solubility (Webster and De Vivo, 2002; Webster et al., 2003; Mathez and Webster, 2005), so the large difference in Cl/K_2O ratios in 79 AD and 1944 AD bulk rocks might reflect pre-eruptive magma composition and pressure condition.
- MIs in olivine and clinopyroxene from cumulates and volcanic rocks show S/Cl depletion (~25% for Group I and 60% for Group II for 79 AD and ~25% for 1944 AD) for both plinian and interplinian events (Table 2 and Fig. 3D). These differences imply that S loss during early fractionation was similar for both AD 79 and 1944 AD magmas.

Experimental studies have determined that S solubility behaviour in silicate melts is complex due to multiple valence states and the occurrence of non-volatile S-rich phases. Sulfur solubility varies as a function of melt composition, especially with Fe content (Carroll and Webster, 1994) and the vapor/melt partition coefficient

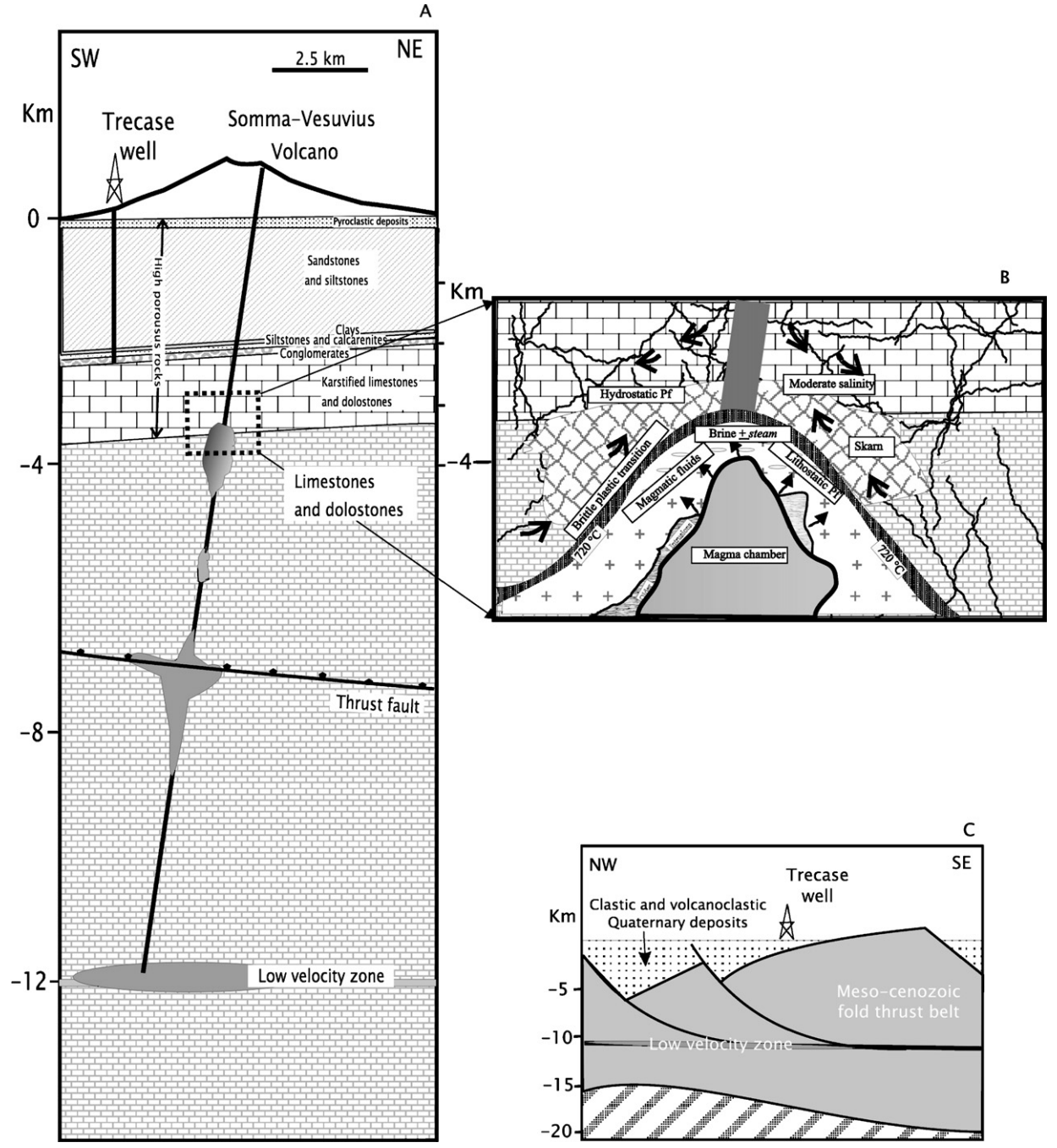

Fig. 6. Stratigraphic successions below Somma–Vesuvius (A), showing also magmatic chambers as in Lima et al. (2003), and below Naples Bay (C) (see Fig. 1 for their location). B) Transition from lithostatic to hydrostatic condition in the Somma–Vesuvius subvolcanic environment. The brittle to plastic transition, consisting of a self-sealed zone, should occur at pressure between 900–1100 bars equivalent to about 3.6–4.5 km depth assuming a temperature of about 720 °C (Fig. 7). Temperature and fluid pressure (P_f) gradients across the interface are very steep. Dilute, dominantly meteoric water circulates at hydrostatic pressure in brittle rock, whereas highly saline brines of magmatic origin accumulate at lithostatic pressure in plastic rock.

for S varies strongly also as a function of both temperature and relative oxygen fugacity (Wallace, 2003 see Fig. 3 pag. 111). At the same oxygen fugacity, S solubility decreases strongly with decreasing temperature, e.g., the partition coefficient increases from about 100 at 900 °C to about a 1000 at 750–780 °C. As a result, magmas may saturate and exsolve an S-rich aqueous volatile phase if the melts evolve to compositions and conditions characterized by lower S solubilities.

As shown in Fig. 3D, even though 1944 AD cumulate olivine phenocrysts have similar Mg# compared with 79 AD cumulate olivine, they are characterized by lower S/Cl content. This observation, along with the evolutionary trend shown in Fig. 4, implies that MIs in 79 AD plinian cumulates were trapped at higher temperature and pressure (considering that magma chambers commonly have a vertical gradient) compared with MIs in 1944 AD interplinian cumulates. On the other hand, Lima et al. (2003) argue that higher concentrations of volatile elements in MIs in primitive phenocrysts suggest crystallization at higher pressure in a deeper magma chamber.

5.1. Differences between plinian (79 AD) and interplinian (1944) hydrothermal system at Somma–Vesuvius

As discussed in the previous section there are marked differences between average volatile contents of MIs as well as in P_2O_5 and Na_2O contents in plinian and interplinian volcanic products. These differences likely represent the effects of hydrothermal activity, when magma resides in the shallow crust and remains a closed system to volatile phase escape for a long time, producing a state of volatile saturation under lithostatic pressure.

During the 1944 AD interplinian activity at Vesuvius, magmas continuously ascended through the system, undergoing simultaneous degassing and fractionation. This could explain part of the Cl/K_2O and S/Cl variations between MIs of 79 AD and 1944 AD cumulates and volcanics and bulk rocks, as discussed in the previous paragraph. The loosely cemented conduit within the volcano did not allow significant build up of volatile pressure, leading to frequent, non-violent inter-plinian eruptions.

This combination of ongoing magma supply and frequent eruptions results in nearly steady-state conditions beneath the volcano, which explains why there is little variation in the composition of the 1944 AD erupting melt (Figs. 2 and 3). The uneven distribution of earlier formed phenocrysts in the ascending magmas (mainly clinopyroxene with subordinate olivine) explains compositional variations observed in the interplinian volcanic rocks (Lima et al., 2003).

These observations, combined with the results of studies of the Somma–Vesuvius hydrothermal system using fluid and saline–melt inclusions, allow us to argue that hydrothermal processes in the Somma–Vesuvius subvolcanic environment, both before and during plinian eruptions, are controlled by the transition from magmatic to hydrothermal conditions (brittle to plastic transition), as described by Fournier (1999).

The 79 AD plinian explosive eruption occurred after a long repose time at closed-conduit conditions. The conduit became closed as a result of cooling of ascending magma at the end of a previous interplinian eruption. As depicted in the model described by Fournier (1999) to explain the formation of epithermal ore deposits associated to porphyry systems, the closing of the system is enhanced by self-sealing processes, such as precipitation of newly formed hydrothermal minerals.

Beneath the Somma–Vesuvius volcanic complex near the upper portion of the shallow magma chamber, a carapace, surrounded by an impermeable rind, forms (and acts as) an interface between the brittle rocks above and plastic rocks below (see also Lima et al., 2006; De Vivo and Lima, 2006). As shown schematically in Fig. 6B, in brittle rock fluids circulate under hydrostatic pressure conditions. In this region, the strain rate needed to cause shear failure of a preexisting open cracks is highly dependent on the coefficient of friction, on fluid pressure (P_f), and on the orientation of the fracture with respect to the stress field (Sibson, 1984). In the plastic rocks at lithostatic pressure conditions (where the least principal stress is the lithostatic load), brine and steam exsolve from crystallizing magma (as in the case of Vesuvius, Webster et al., 2001; Webster and De Vivo, 2002; Webster et al., 2003) and tend to accumulate in thin, overlapping horizontal lenses (Burnham, 1979). In this region the stress difference required to initiate plastic deformation is highly dependent on temperature, strain rate and rock type. When breaches of the self-sealed system occur, and steam and brine are discharged into the brittle, hydrostatically pressured domain, faulting, brecciation, hydrothermal alteration, and vein mineralization occur along with an explosive plinian eruption.

In this scenario, HMIs from 79 AD plinian nodules and from volcanic less evolved crystals (Group I) (Figs. 2 and 3) are trapped in the deeper magma chamber in a state of volatile saturation under lithostatic pressure. More evolved crystal from 79 AD volcanics (Group II) formed in a surficial magma chamber (see Lima et al., 2003) and trapped MIs representing a degassed magma,

in different oxidation state. Note that more evolved clinopyroxene that trapped Group II MIs have been collected in the 79 AD white pumice fallout, which represents the basal products of the eruption.

5.2. Somma–Vesuvius stratigraphic system and brittle-plastic transition zone

The stratigraphic succession below the Somma–Vesuvius volcano (Fig. 6A) has been described by Bernasconi et al. (1981), Milia (1999), Brocchini et al. (2001) and Milia et al. (2003). A carbonatic substrate was encountered at a depth of 1670 mbsl in the Trecase well. The substrate is made up of thrust sheets that involve the Meso–Cenozoic succession and form the Apennine thrust belt. This succession experienced emersion during the Miocene–Pliocene and resulted highly porous rocks in its upper part (approximately 2000 m in thickness) because of karst processes. Successively extensional tectonic activity followed. This tectonic event, occurred during the Pleistocene, was responsible for the formation of a half graben basin bounded by listric faults (Fig. 6C), which merge at ~12 km depth, corresponding to the low velocity zone of Zollo et al. (1998). The Quaternary succession is made up of clastic and volcaniclastic deposits (Fig. 6A).

In particular, the carbonatic rocks are overlain by conglomerates that are in turn covered by 0.98–1.24 Ma-old marine siltstones and calcarenites covered by a thin strata of deep marine clay followed by a succession of marine to subaerial sandstones and siltstones with interbedded lavas and tuffites. A thick pyroclastic succession made up of the Campanian Ignimbrite (39 ka, De Vivo et al., 2001) and pre-Campanian Ignimbrite (Rolandi et al., 2003) was deposited before the volcano formation.

As described in the previous paragraph, several different mechanisms may play a role in triggering major breaches of the self-sealed zone (Fig. 6B). Tectonic activity affected the Vesuvius area before the 79 AD eruption. A tectonic uplift occurring offshore Pompei, predates the deposition of the 79 AD pumice fall (Sacchi et al., 2005). An earthquake, which seriously damaged Pompei, occurred on February 5th 62 AD, with a Magnitude of 5.9 (AAVV, 2004). Because of the high value of the magnitude and of the NW–SE trend of the isosists, we suggest a tectonic origin for the earthquake. We hypothesize that the tectonic event triggered an upward surge of new magma, that 17 years later was responsible of the 79 AD Plinian eruption (see also Hill et al., 2002).

Indeed, the ascending magma temporarily increased the local strain rate to such a degree that previously plastic material underwent shear failure in response to the stress difference. Shear failure allows hypersaline brine and gas to be released quickly from the normally plastic region into the brittle, lower pressure and lower temperature, domain, where hydrothermal veins are deposited as a result of decompression and cooling of the magmatic fluid (Fig. 6B). This mechanism produced skarn type mineralization including chlorides, sulfates and carbonates at Somma–Vesuvius. In particular, fluoride-rich saline fluids led to the formation of accessory Ti-, Zr-, Th-, U- and REE-bearing minerals in vesuvianite skarns (Gilg et al., 2001, Fulignati et al., 2004). Based on data from fluid inclusions in the skarns (Fulignati et al., 2000a; Gilg et al., 2001), the brittle–plastic transition beneath Somma–Vesuvius should occur at 900–1100 bars (3.6–4.5 km dept, Fig. 6B), and at temperature of about 720 °C. Phase relations in the systems NaCl–H_2O and NaCl–KCl–H_2O (Cline and Bodnar, 1994) can provide a good, first approximation of how salinity is likely to vary in Somma–Vesuvius, where hydrothermal fluids exsolved from crystallizing magmas. Precipitation of NaCl occurs when fluid pressure (P_f) is controlled by lithostatic pressure (Fig. 7), at a pressure above 200 bars (about 1 km deep).

5.3. Geochemical variation in volcanic rocks associated with the 79 AD plinian eruption

During plinian events there is a drop in pressure resulting from a breach in the self-sealed zone and magmatic fluid escape into the overlying brittle zone, producing an explosive eruption. The rapid expulsion of steam and brine into overlying, previously hydrostatically pressured part of the system, determines hydraulic fracturing and brecciation (phreatic explosions are likely to occur above the most permeable zone of upward flow).

When fluid pressure (P_f) drops as a result of breaching sealed zone, brine will boil. Brine boiling is important because it may produce a large volume of steam and a coexisting, high salinity brine or vapor plus salt if the pressure drops below about 200 bars (such as in the Vesuvius case) (Fig. 7). At near-magmatic temperatures, decompression from lithostatic to hydrostatic P_f causes brines to become much more saline with the simultaneous evolution of a lower salinity vapor phase.

The shifting of brine into the field of gas (superheated steam)+solid salt at low pressure has important implications regarding the concentrations of HCl that may be transported when (and if) the vapor phase escapes into overlying rock. It is well established that HCl tends to partition into the vapor phase in equilibrium with boiling brine (Candela and Piccoli, 1995; William et al., 1995). This happens because, at pressures

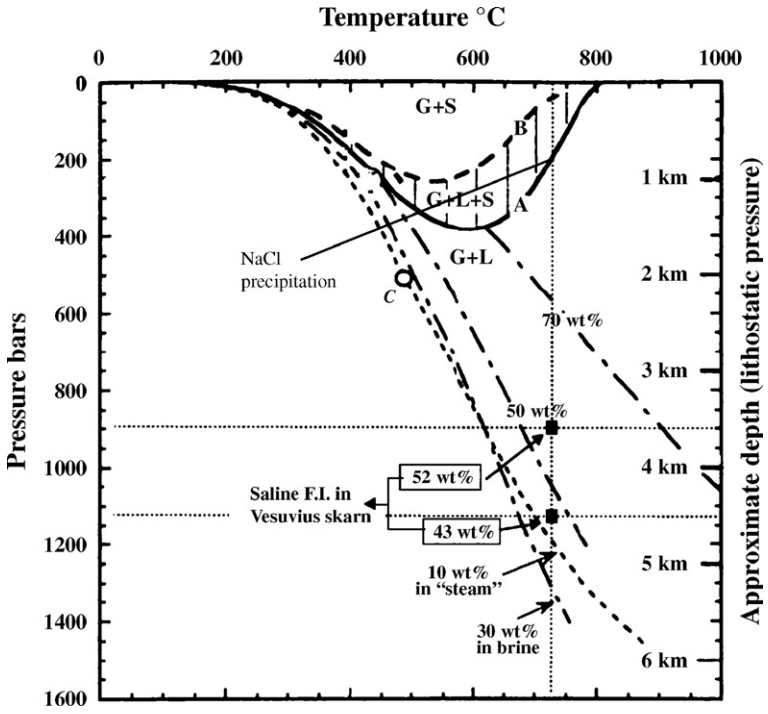

Fig. 7. Temperature–depth diagram showing phase relations in the system NaCl–H_2O with depth corresponding to lithostatic conditions. Multiphase aqueous brine inclusions, yielding salinity between 43 and 53 wt.% NaCl eq., found in Somma–Vesuvius skarn ejecta (Gilg et al., 2001) would be trapped at a pressure between 900–1100 bars, equivalent to about 3.6–4.5 km, assuming a temperature of 720 °C. G = gas; L = liquid; S = solid; dot–dashed lines are contours of constant wt.% NaCl dissolved in brine; short dashed line shows the boiling point curve for a 10 wt.% NaCl solution at pressures and temperatures above its critical point C. Curve A shows the three-phase boundary G+L+S for the system NaCl–H_2O; curve B shows the three-phase boundary G+L+S for the system NaCl–KCl–H_2O, with Na/K in solution fixed by equilibrium with albite and K-feldspar at the indicated temperatures (After Fournier, 1987).

sufficiently low for halite to precipitate, the reaction of NaCl with H_2O become important and hydrolysis reactions produce HCl and NaOH that remain preferentially in the melts (Veksler, 2004).

As discussed above, the greater average Na_2O and Cl content found in 79 AD bulk rocks at Vesuvius could be explained by pre–syn–post eruptive reactions. Fluid migration during cooling and post-emplacement fluid exsolution, can mobilize sufficient material to form a variety of volatile-rich phases like Cl-rich cancrinite, sodalite, halite, and sylvite, as pointed out by Belkin et al. (2006) that identified in massive yellow and gray facies of Campanian Ignimbrite and in piperno: marialitic scapolite containing 4.1 wt.% Cl; cancrinite, containing 8 wt.% Cl (SO_3=4 wt.%); and sodalite containing 7.2 wt.% Cl.

The hydrothermal model could also explain the phosphorus depletion in 79 AD plinian bulk rocks and the loss of other metallic elements. Phosphorus, along with other elements such as Ti, Fe, Mg and Mn, likely forms primary phosphate deposits depending on the physical characteristics of the vapor phase separating from boiling brine during decompression from lithostatic to hydrostatic P_f.

The escape of magmatic fluids from plastic rock at Vesuvius under normal circumstances and without a major perturbing event, is mostly represented by gas (Chiodini et al., 2001; Federico et al., 2002). Likely, during very long repose times, such as the one before the 79 AD plinian eruption, highly differentiated volcanic products were formed by *in situ* processes (exsolution of volatiles at depth and transport to the top of the plutons by convection of the magma) (Shinohara et al., 1995). A necessary condition for volatile transfer to be significant is melt supersaturation with respect to H_2O (Trial and Spera, 1990).

6. Conclusions

Compositions of HMIs in olivine and clinopyroxene (from 79 AD and 1944 AD cumulate nodules and from 79 AD and 1944 AD volcanic rocks) and bulk rock compositions (from 79 AD and 1944 AD eruptions) have been compared to examine differences between the

"closed system" represented by MIs and the "open-system" represented by bulk rocks. P_2O_5/K_2O, Na_2O/K_2O, Cl/K_2O and S/Cl variations between 79 AD and 1944 AD MIs and 79 AD and 1944 AD bulk rocks have been interpreted as being strongly influenced by hydrothermal processes active before, during and post-emplacement explosive eruptions.

During 1944 AD interplinian activity at Vesuvius, magmas continuously ascended through the system, undergoing simultaneous degassing. The loosely cemented conduit within the volcano did not allow significant build up of volatile pressure, leading to frequent, non-violent inter-plinian eruptions. This combination of ongoing magma supply and frequent eruptions results in nearly steady-state conditions under the volcano, which explains why there is little variation in the composition of the 1944 AD erupting melt.

The 79 AD explosive plinian eruption occurs, after a long repose time (similar to all the other plinian eruptions at Vesuvius) at closed-conduit conditions. The latter are created by cooling of magma at the end of previous interplinian eruptions, and are further enhanced by self-sealing processes (precipitation of newly formed minerals) in the waning stage of the active magmatic–hydrothermal system. The above scenario implies that beneath the Somma–Vesuvius volcanic complex, around the upper portion of the shallow magma chamber at a depth between 3.6–4.5 km, a carapace forms and acts as an interface between the brittle and plastic rocks (Fig. 6B). Several different mechanisms may play a role in triggering major breaches of the self-sealed zone. It is likely that the activation of a fault system by a tectonic earthquake in the 62 AD, produced an upward surge of new magma, which after 17 years and immediately before the 79 AD plinian eruption, temporarily increased the local strain rate to such a degree that previously plastic material underwent shear failure in response to a stress difference.

When fluid pressure (P_f) drops as a result of breaching sealed zone, brine will boil producing a large volume of steam and a coexisting, high salinity brine or vapor plus salt if the pressure drops below about 200 bars (Fig. 7). Pre-eruptive reactions (e.g. reaction of NaCl with H_2O) and/or fluid migration during cooling and post-emplacement fluid exsolution that mobilizes sufficient material to form a variety of volatile-rich phases Cl-rich, could explain the greater average Na_2O/K_2O and Cl/K_2O content found in 79 AD volcanic rocks at Vesuvius. Phosphorus, along with other elements such as Ti, Fe, Mg and Mn, forms hydrothermal veins (likely in correspondence of skarn) as a result of decompression and cooling of the magmatic fluid.

Olivine and clinopyroxene HMIs from cumulate nodules collected in 79 AD volcanics and HMIs in olivine from 79 AD volcanics (Group I), were trapped at depth, when the magma was is in a state of volatile saturation. These olivine bearing HMIs from both 79 AD nodules and volcanics experienced common thermal evolution for some time prior to eruption.

The large Cl/K_2O depletion in 1944 bulk rocks reflects pre-eruptive magma conditions as well. During magma fractionation, crystallization of Ca, Mg, Fe, and Al-rich minerals dramatically reduces Cl solubility removing Cl from melt. Chlorine, in addition, escapes from the 1944 AD volcanic system because the latter, in contrast with 79 AD, is in open conduit condition.

Acknowledgments

The authors are very grateful to J. D. Webster for reviewing a preliminary version of the manuscript, and to R. J. Bodnar, L. V. Danyushevsky and H. E. Belkin for their constructive review and helpful suggestions that improved the final version. The research benefited from funds from MIUR-PRIN grants in 2003 and 2004 to B. De Vivo.

References

AAVV, 2004. Catalogo Parametrico Terremoti Italiani. CPTI04, INGV.

Ariskin, A.A., Frenkel, M.Ya., Barmina, G.S., Nielsen, N.L., 1993. COMAGMAT: a Fortran program to model magma differentiation processes. Comput. Geosci. 19, 1155–1170.

Auger, E., Gasparini, P., Virieux, J., Zollo, A., 2001. Seismic evidence of an extended magmatic sill under Mt. Vesuvius. Science 294, 1510–1512.

Ayuso, R.A., De Vivo, B., Rolandi, G., Seal II, R.R., Paone, A., 1998. Geochemical and isotopic Nd–Pb–Sr–O variations bearing on the genesis of volcanic rocks from Vesuvius, Italy. In: Spera, F.J., De Vivo, B., Ayuso, R.A., Belkin, H.E. (Eds.), Vesuvius Special Issue. J. Volcanol. Geotherm. Res., vol. 82, pp. 53–78.

Barberi, M., Leoni, L., 1980. Metamorphic carbonate ejecta from Vesuvius plinian eruptions: evidence of occurrence of shallow magma chambers. Bull. Volcanol. 43, 107–120.

Belkin, H.E., De Vivo, B., 1993. Fluid inclusion studies of ejected nodules from plinian eruptions of Mt. Somma–Vesuvius. In: De Vivo, B., Scandone, R., Trigila, R. (Eds.), Vesuvius Special Issue. J. Volcanol. Geoth. Res., vol. 58, pp. 89–100.

Belkin, H.E., De Vivo, B., Roedder, E., Cortini, M., 1985. Fluid inclusion geobarometry from ejected Mt. Somma–Vesuvius nodules. Am. Mineral. 70, 288–303.

Belkin, H.E., De Vivo, B., Torok, K., Webster, J.D., 1998. Pre-eruptive volatile content, melt-inclusion chemistry, and microthermometry of interplinian Vesuvius lavas (pre-A.D. 1631). In: Spera, F.J., De Vivo, B., Ayuso, R.A., Belkin, H.E. (Eds.), Vesuvius Special Issue. J. Volcanol. Geotherm. Res., 82, pp. 79–95.

Belkin, H.E., De Vivo, B., Lima, A., 2006. Chlorine-Bearing Phases in the Campanian Ignimbrite, Italy. AGU V41A-02, Spring Meet. Baltimore, Abstact.

Bellucci, F., Milia, A., Rolandi, G., Torrente, M.M., 2006. Structural control on the Upper Pleistocene ignimbrite eruptions in the Neapolitan area (Italy): planar volcano tectonic faults versus caldera faults. In: De Vivo (Ed.), Volcanism in the Campania Plain: Vesuvius, Campi Flegrei and Ignimbrites. Developmens in Volcanology, vol. 9. Elsevier Book Series, pp. 165–182.

Bernasconi, A., Bruni, P., Gorla, L., Principe, C., Sbrana, A., 1981. Risultati preliminari dell'esplorazione geotermica profonda nell'area vulcanica del Somma–Vesuvio. Rend. Soc. Geol. Ital. 4, 237–240.

Brocchini, F., Principe, C., Castratori, D., Laurenzi, M.A., Goria, L., 2001. Quaternary evolution of the southern sector of the Campanian Plain and early Somma–Vesuvius activity: insights from the Trecase well. Mineral. Petrol. 73, 67–91.

Brown, P.E., Lamb, W.M., 1989. P–V–T properties of fluids in the system $H_2O \pm CO_2 \pm NaCl$: new graphical presentations and implications for fluid inclusion studies. Geochim. Cosmochim. Acta 53, 1209–1221.

Burnham, C.W., 1979. Magmas and hydrothermal fluids, In: Barnes, H.L. (Ed.), Geochemistry of Hydrothermal Ore Deposits, 2nd ed. Wiley, New York, pp. 31–136.

Candela, P.A., Piccoli, P.M., 1995. Model ore–metal partitioning from melts into vapour and vapour/brine mixtures. Mineral. Assoc. Can. Short Course 23, 101–122.

Carroll, M.R., Webster, J.D., 1994. Solubilities of sulfur, noble gas, nitrogen, chlorine, and fluorine in magmas. Rev. Miner. 30, 231–279.

Chiodini, G., Marini, L., Russo, M., 2001. Geochemical evidence for the existence of high-temperature hydrothermal brines at Vesuvio volcano, Italy. Geochim. Cosmochim. Acta 65, 2129–2147.

Cioni, R., 2000. Volatile content and degassing processes in the AD 79 magma chamber at Vesuvius (Italy). Contrib. Mineral. Petrol. 140, 40–54.

Cline, J.S., Bodnar, R.J., 1994. Direct evolution of brine from crystallizing silicic melt at the Questa, New Messico, molybdenum deposit. Econ. Geol. 89, 1780–1802.

Cortini, M., Hermes, O.D., 1981. Sr isotopic evidence for a multi-source origin of the potassic magmas in the Neapolitan area S. Italy. Contrib. Mineral. Petrol. 77, 47–55.

Cortini, M., Lima, A., De Vivo, B., 1985. Trapping temperatures of melt inclusions from ejecta Vesuvian mafic xenoliths. J. Volcanol. Geotherm. Res. 26, 167–172.

Danyushevsky, L.V., 2001. The effect of small amounts of H_2O on crystallisation of mid-ocean ridge and backarc basin magmas. J. Volcanol. Geotherm. Res. 110, 265–280.

Danyushevsky, L.V., Della-Pasqua, F.N., Sokolov, S., 2000. Re-equilibration of melt inclusions trapped by magnesian olivine phenocrysts from subduction-related magmas: petrological implications. Contrib. Mineral. Petrol. 138, 68–83.

Danyushevsky, L.V., Sokolov, S., Falloon, T.J., 2002. Melt inclusions in olivine phenocrysts: using diffusive re-equilibration to determine the cooling history of a crystal, with implications for the origin of picrites and other olivine–phyric rocks. J. Petrol. 43 (9).

De Vivo, B., Lima, A., 2006. A hydrothermal model for ground movements (bradyseism) at Campi Flegrei, Italy. In: De Vivo (Ed.), Volcanism in the Campania Plain: Vesuvius, Campi Flegrei and Ignimbrites. Developmens in Volcanology, vol. 9. Elsevier Book Series, pp. 291–319.

De Vivo, B., Cortini, M., Belkin, H.E., Roedder, E., 1982. Inclusion geobarometry from ejected mafic Vesuvian xenoliths. Geol. Soc. Am., Abstr. Programs 14, 474.

De Vivo, B., Rolandi, G., Gans, P.B., Calvert, A., Bohrson, W.A., Spera, F.J., Belkin, H.E., 2001. New constraints on the pyroclastic eruptive history of the Campania volcanic Plain (Italy). Mineral. Petrol. 73, 47–65.

Dolfi, D., Trigila, R., 1978. The role of water in the 1944 Vesuvius eruption. Contrib. Mineral. Petrol. 67, 97–304.

Einaudi, M.T., Meinert, L.D., Newberry, R.J., 1981. Skarn Deposits. Econ. Geol. 75th Anniv. Vol. 317–391.

Federico, C., Aiuppa, A., Allard, P., Bellomo, S., Jean-Baptiste, P., Parello, F., Valenza, M., 2002. Magma-derived gas influx and water–rock interactions in the volcanic aquifer of Mt. Vesuvius, Italy. Geochim. Cosmochim. Acta 66, 963–981.

Ford, C.E., Russell, D.G., Craven, J.A., Fisk, M.R., 1983. Distribution coefficients of Mg^{2+}, Fe^{2+}, Ca^{2+} and Mn^{2+} between olivine and melt. J. Petrol. 24, 256–265.

Fournier, R.O., 1987. Conceptual models of brine evolution in magmatic–hydrothermal systems. U. S. Geol. Surv. Prof. Pap. 1350. 2, 1487–1506.

Fournier, R.O., 1999. Hydrothermal processes related to movement of fluid from plastic into brittle rock in the magmatic–epithermal environment. Econ. Geol. 94 (8), 1193–1212.

Fulignati, P., Marianelli, P., Sbrana, A., 1998. New insights on the thermometamorphic–metasomatic magma chamber shell of the 1944 eruption of Vesuvius. Acta Volcanol. 10, 47–54.

Fulignati, P., Marianelli, P., Santacroce, R., Sbrana, A., 2000a. The skarn shell of the 1944 Vesuvius magma chamber. Genesis and P–T–X conditions from melt and fluid inclusion data. Eur. J. Mineral. 12, 1025–1039.

Fulignati, P., Marianelli, P., Sbrana, A., 2000b. Glass bearing felsic nodules from crystallizing side walls of 1944 Vesuvius magma chamber. Mineral. Mag. 64, 481–496.

Fulignati, P., Kamenetsky, V.S., Marianelli, P., Sbrana, A., Mernagh, T.P., 2001. Melt inclusion record of immicibility between silicate, hydrosaline, and carbonate melts: applications to skarn genesis at Mount Vesuvius. Geology 29, 1043–1046.

Fulignati, P., Marianelli, P., Santacroce, R., Sbrana, A., 2004. Probing the Vesuvius magma chamber–host rock interface through xenoliths. Geol. Mag. 141, 417–428.

Gilg, H.A., Lima, A., Somma, R., Ayuso, R.A., Belkin, H.E., De Vivo, B., 1999. A fluid inclusion and isotope study of calc-silicate ejecta from Mt. Somma–Vesuvius: evidence for interaction of high-temperature hypersaline fluids with the sedimentary basement. Proceedings of ECROFI XV, Potsdam, Germany, Abstracts and Program. Terra nostra, vol. 99(6), pp. 118–120.

Gilg, H.A., Lima, A., Somma, R., Belkin, H.E., De Vivo, B., Ayuso, R. A., 2001. Isotope geochemitry and fluid inclusion study of skarns from Vesuvius. Mineral. Petrol. 73, 145–176.

Hermes, O.D., Cornell, W.C., 1978. Petrochemical significance of xenolithic nodules associated with potash-rich lavas of Somma–Vesuvius volcano. NSF Final Technical Report, Univ. of Rhode Island.

Hermes, O.D., Cornell, W.C., 1981. Quenched crystal mush and associated magma compositions as indicated by intercumulus glasses. J. Volcanol. Geotherm. Res. 9, 133–149.

Hermes, O.D., Cornell, W.C., 1983. The significance of mafic nodules in the ultrapotassic rocks from Central Italy — reply. J. Volcanol. Geotherm. Res. 16, 166–172.

Hill, D.P., Pollitz, F., Newhall, C., 2002. Earthquake–volcano interactions. Phys. Today 41–47 (November).

Kwak, T.A.P., 1986. Fluid inclusions in skarns carbonate replacement deposits. J. Metamorph. Petrol. 4, 363–384.

Lima, A., 2000. Experimental study on melt inclusions in clinopyroxene phenocrystals from Roccamonfina lavas Italy. Mineral. Petrol. 70, 199–220.

Lima, A., Danyushevsky, L.V., De Vivo, B., Fedele, L., 2003. A model for the evolution of the Mt. Somma–Vesuvius magmatic system based on fluid and melt inclusion investigations. In: De Vivo, B., Bodnar, R.J. (Eds.), Melt Inclusions in Volcanic Systems: Methods, Applications and Problems. Developmens in Volcanology, vol. 5. Elsevier Book Series, pp. 227–249.

Lima, A., De Vivo, B., Fedele, L., Sintoni, F., 2006. Influence of hydrothermal precesses on geochemical variations between 79 AD and 1944 AD Vesuvius eruption. In: De Vivo (Ed.), Volcanism in the Campania Plain: Vesuvius, Campi Flegrei and Ignimbrites. Developmens in Volcanology, vol. 9. Elsevier Book Series, pp. 237–349.

Marianelli, P., Métrich, N., Santacroce, R., Sbrana, A., 1995. Mafic magma batches at Vesuvius: a glass inclusion approach to the modalities of feeding stratovolcanoes. Contr. Mineral. Petrol. 120, 159–169.

Marianelli, P., Metrich, N., Sbrana, A., 1999. Shallow and deep reservoirs involved in magma supply of the 1944 eruption of Vesuvius. Bull. Volcanol. 61, 48–63.

Marsh, B.D., 1995. Solidification fronts and magmatic evolution. Mineral. Mag. 60, 5–40.

Mathez, E.A., Webster, J.D., 2005. Partitioning behaviour of chlorine and fluorine in the system apatite–silicate melt–fluid. Geochim. Cosmochim. Acta 69, 1275–1286.

Meinert, L.D., Hefton, K.K., Mayers, D., Tasiran, I., 1997. Geology, zonation, and fluid evolution of the BigGossan Cu–Au skarn deposit, Ertsberg district, Irian Java. Econ. Geol. 92, 509–534.

Milia, A., 1999. Aggrading and prograding infill of a pery-Tyrrhenian basin (Naples Bay, Italy). Geo Mar. Lett. 19, 73–88.

Milia, A., Torrente, M.M., 1999. Tectonics and stratigraphic architecture of a pery-Tyrrhenian half-graben (Bay of Naples, Italy). Tectonophysics 315, 297–314.

Milia, A., Mirabile, L., Torrente, M.M., Dvorak, J.J., 1998. Volcanism offshore of Vesuvius volcano in Naples Bay. Bull. Volcanol. 59, 404–413.

Milia, A., Torrente, M.M., Russo, M., Zuppetta, A., 2003. Tectonics and crustal structure of the Campania continental margin: relationships with volcanism. Mineral. Petrol. 79, 33–47.

Raia, F., Webster, J.D., De Vivo, B., 2000. Pre-eruptive volatile contents of Vesuvius magmas: constraints on eruptive history and behavior. I. The medieval and modern interplinian activities. Eur. J. Mineral. 12, 179–193.

Roedder, E., 1979. Origin and significance of magmatic inclusions. Bull. Mineral. 102, 487–510.

Rolandi, G., Petrosino, P., McGeehin, J., 1998. The interplinian activity of Somma–Vesuvius in the last 3500 years. In: Spera, F.J., De Vivo, B., Ayuso, R.A., Belkin, H.E. (Eds.), Vesuvius Special Issue. J. Volcanol. Geotherm. Res., vol. 82, pp. 19–52.

Rolandi, G., Bellucci, F., Heizler, M.T., Belkin, H., De Vivo, E., 2003. Tectonic controls on the genesis of ignimbrites from the Campanian Volcanic Zone, Southern Italy. In: De Vivo, B., Scandone, R. (Eds.), Ignimbrites of the Campanian Plain, Italy. Mineralogy and Petrology, vol. 79, pp. 3–31.

Sacchi, M., Insinga, D., Milia, A., Molosso, F., Raspini, A., Torrente, M.M., Conforti, A., 2005. Stratigraphic signature of the Vesuvius 79 AD event off the Sarno prodelta system, Naples Bay. In: Trincardi, F., Syvitski, J. (Eds.), Mediterranean Prodelta Systems. Marine Geology, vol. 222–223, pp. 443–469. Special Issue C.

Santacroce, R., Bertagnini, A., Civetta, L., Landi, P., Sbrana, A., 1993. Eruptive dynamics and petrogenetic processes in a very shallow magma reservoir: the 1906 eruption of Vesuvius. J. Petrol. 34, 383–425.

Scandone, R., Giacomelli, L., Gasparini, P., 1993. Mount Vesuvius: 2000 years of volcanological observations. J. Volcanol. Geotherm. Res. 58, 5–25.

Shinohara, H., Kazahaya, K., Lowenstern, J.B., 1995. Volatile transport in a convecting magma column: implications for porphyry Mo mineralization. Geology 23, 1091–1094.

Sibson, R.H., 1984. Roughness at the base of the seismogenic zone: contributing factors. J. Geophys. Res. 89, 5791–5799.

Sintoni, M.F., Lima, A., Webster, J.D., De Vivo, B., 2005. Sulfur and chlorine behavior during the last three plinian eruptions of Mt.Somma–Vesuvius. Eos Trans. AGU 86 (52) (Fall Meet. Suppl., Abstract.).

Sobolev, A.V., Slutskii, A.B., 1984. Composition and crystallization conditions of the initial melt of the Siberian meimechites in relation to the general problem of ultrabasic magmas. Sov. Geol. Geophys. 25, 93–104.

Thomas, J.B., Bodnar, R.J., 2002. A technique for mounting and polishing melt inclusions in small <1 mm crystals. Am. Mineral. 87, 1505–1508.

Trial, A.F., Spera, F.J., 1990. Mechanisms for the generation of compositional heterogeneities in magma chamber. Geol. Soc. Amer. Bull. 102, 353–367.

Veksler, I.V., 2004. Liquid immiscibility and its role at magmatic–hydrothermal transition: a summary of experimental studies. Geochem. Geol. 210, 7–31.

Wallace, P., 2003. From magma to atmosphere: magma degassing, explosive eruptions, and volcanic volatile budgets. In: De Vivo, B., Bodnar, R.J. (Eds.), Melt Inclusions in Volcanic Systems: Methods, Applications and Problems. Developmens in Volcanology, vol. 5. Elsevier Book Series, pp. 105–127.

Webster, J.D., De Vivo, B., 2002. Experimental and modeled solubilities of chlorine in aluminosilicate melts. Consequences of magma evolution, and implications for magmatic brine exsolution at Mt. Somma–Vesuvius. Am. Mineral. 87, 1046–1061.

Webster, J.D., Raia, F., De Vivo, B., Rolandi, G., 2001. The behavior of chlorine and sulfur during differentiation of the Mt. Somma–Vesuvius magmatic system. Mineral. Petrol. 73, 177–200.

Webster, J.D., De Vivo, B., Tappen, C., 2003. Volatiles, magmatic degassing and eruptions of Mt. Somma–Vesuvius: constraints from silicate melt inclusions, solubility experiments and modeling. In: De Vivo, B., Bodnar, R.J. (Eds.), Melt Inclusions in Volcanic Systems: Methods, Applications and Problems. Developmens in Volcanology, vol. 5. Elsevier Book Series, pp. 207–226.

William, T.J., Candela, P.A., Piccoli, P.M., 1995. The partitioning of copper between silicate melt and two-phases aqueous fluids: an experimental investigation at 1 kbar, 800 °C and 0.5 kbar, 859 °C. Contrib. Mineral. Petrol. 121, 388–399.

Zambonini, F., 1910. Mineralogia Vesuviana. Atti R. Accad. Sci. Fis., Mat. Ser. 2° 14 (7), 1–463.

Zollo, A., Gasparini, P., Virieux, J., Biella, G., Boschi, E., Captano, P., de Franco, R., Dell'aversana, P., de Matteis, R., De Natale, G., Jannaccone, G., Guerra, I., Le Meur, H., Mirabile, L., 1998. An image of Mt. Vesuvius obtained by 2D seismic tomography. J. Volcanol. Geotherm. Res. 82, 161–173.